

### **PAPER**

# Electron transport in ZnMgO/ZnO heterostructures

To cite this article: Qun Li et al 2014 Semicond. Sci. Technol. 29 115001

View the article online for updates and enhancements.

# You may also like

- Comparative study of ZnMgO/GaAs and ZnMgO/Si solar cells
   Wei Zhang and Naiyun Tang
- Micro-mechanism study of the effect of Cd-free buffer layers ZnXO (X = Mg/Sn) on the performance of flexible Cu<sub>2</sub>ZnSn(S, Se)<sub>4</sub> solar cell Caixia Zhang, , Yaling Li et al.
- Vapour-liquid-solid growth of ZnO-ZnMgO core—shell nanowires by gold-catalysed molecular beam epitaxy
   W Kennedy, E R White, M S P Shaffer



Semicond. Sci. Technol. 29 (2014) 115001 (7pp)

doi:10.1088/0268-1242/29/11/115001

# Electron transport in ZnMgO/ZnO heterostructures

Qun Li<sup>1</sup>, Jingwen Zhang<sup>1</sup>, Zhiyun Zhang<sup>2</sup>, Fengnan Li<sup>1</sup> and Xun Hou<sup>1</sup>

E-mail: jwzhang@mail.xjtu.edu.cn

Received 9 March 2014, revised 8 July 2014 Accepted for publication 15 July 2014 Published 20 August 2014

### **Abstract**

We numerically calculate the wave function of two-dimensional electron gas (2DEG) for use in 2DEG transport theory and study the electron transport in ZnMgO/ZnO heterostructures. For strongly confined 2DEG, the temperature dependence of the electron mobility is satisfactorily explained using 2DEG transport theory. The interface roughness and ionized impurity scatterings play important roles in the electron transport at low and moderate temperatures. At room temperatures polar optical phonon scattering is the most important scattering mechanism. For heterostructures having two parallel conduction paths in the 2DEG at the ZnMgO/ZnO interface and in the ZnO thick layer, the electron transport is contributed by the two paths. We calculate the mobility for the respective conduction paths, and then combine the two mobility components to fit the experimental data. The theoretical calculations are in good agreement with the experimental data.

Keywords: II-VI semiconductors, ZnMgO/ZnO heterostructures, electron transport, parallel conduction

(Some figures may appear in colour only in the online journal)

# 1. Introduction

Zinc oxide-based materials have been widely used for production of optoelectronic devices covering the UV and the visible range, due to the direct ZnO gap of 3.4 eV and the large excitonic ZnO binding energy of 60 meV [1–3]. A two-dimensional electron gas (2DEG) with a high sheet carrier density (over  $1.0 \times 10^{13}$  cm<sup>-2</sup>) and a high mobility (over  $1.0 \times 10^5$  cm<sup>2</sup>/Vs) can form at the ZnMgO/ZnO interface, which shows the great potential of ZnMgO/ZnO heterostructures in high-power, high-frequency applications [2, 4–6].

The wave function of 2DEG describes the electron distribution perpendicular to the 2DEG plane, which is closely related to the theoretical predictions of the heterostructure properties. The analytical wave functions proposed by Fang and Howard [7] and Ando [8] have been used extensively in

various heterostructure systems [9–11], because of their mathematical simplicity. But the Fang–Howard and Ando wave functions may not work well in describing electron penetration into the barrier layer. In calculations of transport properties in wurtzite heterostructures, numerical 2DEG wave functions are preferred over the analytical ones.

Undoped ZnO films always exhibit n-type conductivity with background electron densities between 10<sup>16</sup> and 10<sup>17</sup> cm<sup>-3</sup> [12], which is believed to be caused by native point defects [13]. In real ZnMgO/ZnO heterostructures, the sheet carrier density of defects-induced bulk electrons in the ZnO thick layer can be comparable to, and may even exceed, the sheet carrier density of 2DEG at the ZnMgO/ZnO interface. In this situation, there are two parallel conduction paths in the 2DEG and in the three-dimensional (3D) ZnO thick layer. The 2DEG and bulk conduction both contribute to the electron transport in ZnMgO/ZnO heterostructures. The electron

<sup>&</sup>lt;sup>1</sup> Key Laboratory for Physical Electronics and Devices of the Ministry of Education, Key Laboratory of Photonics Technology for Information of Shaanxi Province, and ISCAS-XJTU Joint Laboratory of Functional Materials and Devices for Informatics, School of Electronics and Information Engineering, Xi'an Jiaotong University, Xi'an 710049, China

<sup>&</sup>lt;sup>2</sup> School of Materials Science and Engineering, Xi'an University of Science and Technology, Xi'an 710054, China

transport in bulk ZnO and in ZnMgO/ZnO heterostructures have been studied using pure bulk and 2DEG transport theories [14–16], respectively, but studies on the effect of parallel conduction on the electron transport in ZnMgO/ZnO heterostructures have not been reported.

In this study, we numerically calculate the wave function of the 2DEG and study the electron transport in ZnMgO/ZnO heterostructures. An electrostatic model taking into account all possible charge sources is built to calculate the 2DEG wave function using a numerical method. A scattering theory for the 2DEG is described, and is applied to fit the 2DEG mobility reported by Tampo *et al* [6]. The electron mobilities in ZnO/ZnMgO heterostructures reported by Tsukazaki *et al* [5] are successfully explained by a parallel conduction mechanism.

# 2. Theory

### 2.1. Wave function of 2DEG

2.1.1. Electrostatic model. A typical Zn-polar ZnMgO/ZnO heterostructure consists of a fully strained ZnMgO (0001) barrier layer and a fully relaxed ZnO (0001) buffer layer. The spontaneous and piezoelectric polarization effects induce a 2DEG at the ZnO side of the ZnMgO/ZnO interface. Here the ZnO c-axis [0001] is defined as z-axis; the ZnMgO and ZnO layers occupy the regions z < 0 and z > 0, respectively. The energy level  $E_i$  and wave function  $\zeta_i(z)$  of electrons in the 2DEG obey the Schrödinger equation,

$$-\frac{\hbar^2}{2 m^*} \frac{d^2}{dz^2} \zeta_i(z) + V(z)\zeta_i(z) = E_i \zeta_i(z), \tag{1}$$

where  $\hbar$  is the reduced Planck constant,  $m^*$  is the electron effective mass, and V(z) is the potential energy. The potential energy V(z) is given by

$$V(z) = -e\phi(z) + \Delta E_c \Theta(-z), \qquad (2)$$

where e is the electronic charge,  $\Theta(z)$  is the step function,  $\Delta E_c = 0.9 \times \Delta E_g$  is the conduction band discontinuity at the ZnMgO/ZnO interface,  $\Delta E_g$  is the band gap discontinuity of 2.145x eV for an Mg composition x [17], and the electrostatic potential  $\phi(z)$  satisfies the Poisson equation,

$$-\varepsilon_0 \frac{\mathrm{d}}{\mathrm{d}z} \left[ \varepsilon_{\mathrm{s}} \frac{\mathrm{d}}{\mathrm{d}z} \phi \right] = \sigma_{\mathrm{s}} \delta(z+d) - \sigma_{\mathrm{t}} \delta(z+d) + \sigma_{\mathrm{i}} \delta(z) + n_{\mathrm{d}} - n_{\mathrm{e}}(z),$$
(3)

where  $\varepsilon_0$  is the permittivity of free space,  $\varepsilon_s$  is the low frequency permittivity, d is the ZnMgO barrier width,  $\delta(z)$  is the delta function. The source terms on the right side of (3) takes into account ionized surface states and polarization charge at the ZnMgO surface, polarization charge at the ZnMgO/ZnO interface, ionized donors throughout the heterostructure, and electrons in the 2DEG channel. Donor-like surface states on the ZnMgO (0001) surface are regarded as the main source of the 2DEG electrons [17, 18]. After releasing electrons to the 2DEG, ionized surface states with a

sheet charge density  $\sigma_s$  are left at the surface (z = -d). For Zn-polar ZnMgO/ZnO heterostructures, the polarization charge at the bottom surface of the ZnO layer has a sheet density  $\sigma_b = 0.054 \text{ C/m}^2$  [19], but this charge component is assumed to be fully screened and thus is not included in (3); if not, the 2DEG cannot form at the ZnMgO/ZnO interface. Spontaneous and piezoelectric polarizations induced sheet charge density at the ZnMgO/ZnO interface (z = 0) is  $\sigma_i = 0.024x \text{ C/m}^2$  for an Mg composition x [20]. Because the total polarization charges must maintain electric neutrality, the polarization sheet charge density at the ZnMgO (0001) surface (z = -d) is  $\sigma_t = -0.054 - 0.024x \text{ C/m}^2$ . In this work the electric quantum limit is assumed, i.e. all electrons in the 2DEG occupy the first subband. Therefore, the charge density of the 2DEG is given by  $n_e(z) = e \cdot N_s^{(2D)} \cdot |\zeta_1(z)|^2$ , here  $N_s^{(2D)}$  is the 2DEG sheet carrier density and  $\zeta_1(z)$  is the first subband wave function. Ionized donor impurities are assumed to have a uniform density  $N_{\rm IM}$  throughout the heterostructure, thus the charge density of ionized donors is  $n_{\rm d} = e \cdot N_{\rm IM}$ . All charge components involved in (3) should maintain charge neutrality across the ZnMgO layer and the electron channel region, thus

$$\int_{-\infty}^{\infty} \left[ \sigma_{s} \delta(z+d) - \sigma_{t} \delta(z+d) + \sigma_{i} \delta(z) + n_{d} - n_{e}(z) \right] dz = 0.$$
(4)

2.1.2. Numerical method. A self-consistent solution of the Schrödinger and Poisson equations can be obtained using a numerical iterative method, details of the calculations can be found elsewhere [21, 22]. To solve the Poisson equation, two boundary conditions imposed on the electrostatic model are that the electrostatic potential at the ZnMgO/ZnO interface is zero (i.e.  $\phi(0) = 0$ ), and the electrostatic field inside the ZnO layer is zero (i.e.  $\phi'(\infty) = 0$ ).

Tsukazaki *et al* [5] estimated the polarization charge distribution in O-polar ZnO/ZnMgO heterostructures. With these estimates, the self-consistent calculations can be performed on O-polar ZnO/ZnMgO heterostructures.

# 2.2. Scattering mechanisms in 2DEG

The scattering theories of the 2DEG system have been well developed by several authors [9, 15, 23–25]. We give below a brief description of the most important scattering mechanisms, i.e. alloy scattering, interface roughness scattering, ionized impurity scattering, acoustic phonon scattering, and polar optical phonon scattering. All interactions between electrons and these scattering mechanisms (except polar optical phonons) are regarded as elastic collisions, thus an analytical momentum relaxation time  $\tau(E)$  can be defined.

The energy average of  $\tau(E)$  is given by [9]

$$\langle \tau(E) \rangle = \frac{\int \tau(E) E \left[ \frac{\mathrm{d}f_0(E)}{\mathrm{d}E} \right] \mathrm{d}E}{\int E \left[ \frac{\mathrm{d}f_0(E)}{\mathrm{d}E} \right] \mathrm{d}E}, \tag{5}$$

where  $f_0(E) = 1/\{\exp[(E - E_{\rm F})/k_{\rm B}T] + 1\}$  is the Fermi–Dirac function,  $E_{\rm F}$  is the Fermi level,  $k_{\rm B}$  is the Boltzmann constant, and T is the temperature.

2.2.1. Alloy scattering (ALS). In ZnMgO, the random distribution of cations destroys the crystal periodic potential and thus causes a perturbation on electron motion, which is termed the ALS. The electrons penetrating into the ZnMgO layer will suffer strong ALS because of large conduction band offset between MgO and ZnO. The matrix element for the ALS is given by [24, 26]

$$\left| M_{\text{ALS}} \right|^2 = \frac{1}{S} \Omega x (1 - x) (\Delta V)^2 \int_{-d}^0 \left| \zeta_1(z) \right|^4 dz, \tag{6}$$

where S is the sample area, x is the Mg composition of the ZnMgO layer,  $\Omega = \sqrt{3} \, a^2(x) c(x)/2$  is the volume of a ZnMgO unit cell, a(x) = 0.3250 + 0.005x nm and c(x) = 0.5204 - 0.017x nm are lattice constants of the ZnMgO [27]. The conduction band offset  $\Delta V$  is assumed to be half the band-gap difference between ZnO and MgO:  $\Delta V = [E_{\rm g}({\rm MgO}) - E_{\rm g}({\rm ZnO})]/2$ 

= (6.4 - 3.43)/2 = 1.49 eV [28]. The reciprocal momentum relaxation time is given by

$$\frac{1}{\tau_{\text{ALS}}(E)} = \frac{m^* \Omega x (1 - x) (\Delta V)^2}{\pi \hbar^3} \times \int_0^{\pi} \left[ \int_{-d}^0 \left| \zeta_1(z) \right|^4 dz \right] \frac{(1 - \cos \theta)}{\epsilon^2(a)} d\theta, \tag{7}$$

where  $\theta$  is the angle between electron wave vectors before and after scattering. In the zero-temperature random phase approximation, the screening function  $\epsilon(q)$  is written as [9]

$$\epsilon(q) = 1 + \frac{e^2 m^*}{2\pi \hbar^2 \epsilon_0 \epsilon_s} H(q), \tag{8}$$

where q is the component of 3D wave vector parallel to the 2DEG plane. q is related to the electron wave vector k by the relation  $q = 2k \sin(\theta/2)$ . The form factor H(q) is written as

$$H(q) = \int dz \int dz' \zeta_1^2(z) \zeta_1^2(z') \exp(-q|z-z'|).$$
 (9)

The screening function as shown in (8) is also employed in other scattering mechanisms.

2.2.2. Interface roughness scattering (IRS). IRS may play an important role in the electron transport in a 2DEG. However, interface roughness is difficult to directly measure and to accurately model, because the fluctuations in the interface position are spatially random. In theoretical calculations, two analytical correlation functions, i.e. for the Gaussian,  $C(r) = \Delta^2 \exp\left(-r^2/\Lambda^2\right)$ , and exponential,

 $C(r) = \Delta^2 \exp(-r/\Lambda)$  [29], have usually been employed to describe the statistical properties of interface roughness for simplifying the scattering model. Which form is the better approximation depends on real interface profile. Once one form has been fixed, the interface roughness can be described by two parameters, i.e. the average roughness height  $\Delta$ , and the horizontal correlation length  $\Lambda$ . In this study we assume the exponential distribution; thus the matrix element for the IRS is given by [29]

$$|M_{\rm IRS}|^2 = \frac{e^4 \Delta^2 \Lambda^2 \left[ N_{\rm s}^{(2D)} \right]^2}{2S \varepsilon_0^2 \varepsilon_{\rm s}^2} \left( 1 + q^2 \Lambda^2 \right)^{-\frac{3}{2}}.$$
 (10)

The reciprocal momentum relaxation time is given by

$$\frac{1}{\tau_{\text{IRS}}(E)} = \frac{e^4 m^* \Delta^2 \Lambda^2 \left[ N_s^{\text{(2D)}} \right]^2}{2\pi \hbar^3 \varepsilon_0^2 \varepsilon_s^2} \times \int_0^{\pi} \left( 1 + q^2 \Lambda^2 \right)^{-\frac{3}{2}} \frac{1 - \cos \theta}{\varepsilon^2(q)} d\theta. \tag{11}$$

2.2.3. Ionized impurity scattering (IIS). Most ZnMgO/ZnO heterostructures are grown without intentional doping, but residual impurities cannot be completely removed. Residual impurities can cause local deformations of the crystal lattice; further, ionized residual impurities can affect electron mobility via Coulomb interactions. The lattice deformation scattering is quite small compared with the Coulomb scattering [30], therefore, only the IIS is taken into account in the impurity scattering. In the Brooks–Herring model, the matrix element for the IIS is given by [24]

$$|M_{\rm HS}|^2 = \frac{e^4 N(z) [F_{\rm c}(q,z)]^2}{4S \varepsilon_0^2 \varepsilon_z^2 a^2},$$
 (12)

where N(z) is the density of ionized impurities,  $F_{\rm c}(q,z)$  is given by

$$F_{c}(q, z) = \int dz' |\zeta_{1}(z')|^{2} \exp(-q|z - z'|).$$
 (13)

We assume that ionized impurities are uniformly distributed in the heterostructure at a density of  $N_{\rm IM}$ , thus the reciprocal momentum relaxation time can be written as

$$\frac{1}{\tau_{\text{IIS}}(E)} = \frac{e^4 \, m^* N_{\text{IM}}}{4\pi \hbar^3 \varepsilon_0^2 \, \varepsilon_s^2} \times \int_0^{\pi} \frac{\int \left[ F_{\text{c}}(q, z) \right]^2 dz}{q^2 \varepsilon^2(q)} (1 - \cos \theta) d\theta. \tag{14}$$

2.2.4. Acoustic phonon scattering. Acoustic phonon scattering may be important at low and moderate temperatures, particularly in the materials of high purity with low defect density. Because wurtzite ZnO has a noncentrosymmetric structure, the electron-acoustic phonon interactions arise from both deformation-potential (DP) and piezoelectric (PE) coupling. In calculations, we neglect the

**Table 1.** Parameters of ZnO employed in calculations. Here  $m_0$  is the free electron mass.

Parameter	Symbol (units)	Value
Mass density	$\rho$ (g/cm <sup>3</sup> )	5.67 <sup>a</sup>
Electron effective mass	$m^*$	$0.3m_0^{\ b}$
High frequency permittivity	$arepsilon_{ m h}$	3.7°
Low frequency permittivity	$arepsilon_{ ext{S}}$	7.9°
LA-phonon velocity	$u_1 \text{ (m/s)}$	$5.0 \times 10^{3d}$
PO-phonon temperature	$T_{PO}(K)$	837 <sup>e</sup>
Piezoelectric tensor	$e_{15} (\text{C/m}^2)$	$-0.37^{f}$
	$e_{31}$ (C/m <sup>2</sup> )	$-0.62^{f}$
	$e_{33} (\text{C/m}^2)$	0.96 <sup>f</sup>
Acoustic DP constant	D (eV)	15 <sup>g</sup>

a [32]

acoustic phonon energy, and approximate the phonon distribution by the equipartition law. A detailed description of the acoustic phonon scattering can be found in [9] and [31].

2.2.5. Polar optical (PO) phonon scattering. An analytical expression for the momentum relaxation time for PO phonon scattering cannot be strictly defined because the PO phonon scattering is both anisotropic and inelastic. Solving the Boltzmann equation directly is necessary for the accurate treatment of the PO phonon scattering. Applying the Boltzmann equation to the PO phonon scattering, one can get [9]

$$1 = S_0(E)\Phi(E) - S_a(E)\Phi(E + \hbar\omega_0) - S_e(E)\Phi(E - \hbar\omega_0),$$
 (15)

here  $S_0$  is the out-scattering rate,  $S_a$  and  $S_e$  are the in-scattering rates for absorption and emission processes of the PO phonons, respectively,  $\Phi(E)$  is the perturbation term to be determined. Detailed expressions of  $S_0$ ,  $S_a$ , and  $S_e$  can be found in [9]. In this study an iterative method is used to solve (15). Once  $\Phi(E)$  is obtained, the momentum relaxation time can be calculated from (5) by replacing  $\tau(E)$  by  $\Phi(E)$ . If  $S_0$  is the sum of the out-scattering rate of PO scattering and total elastic scattering rates, a result contributed by all scattering processes can be obtained.

The physical parameters used in the calculations below are listed in table 1.

# 3. Calculated results and discussion

# 3.1. Calculated 2DEG wave functions

Figure 1 shows the 2DEG wave functions calculated numerically for three different cases. In the electric quantum limit, the 2DEG wave functions are independent of

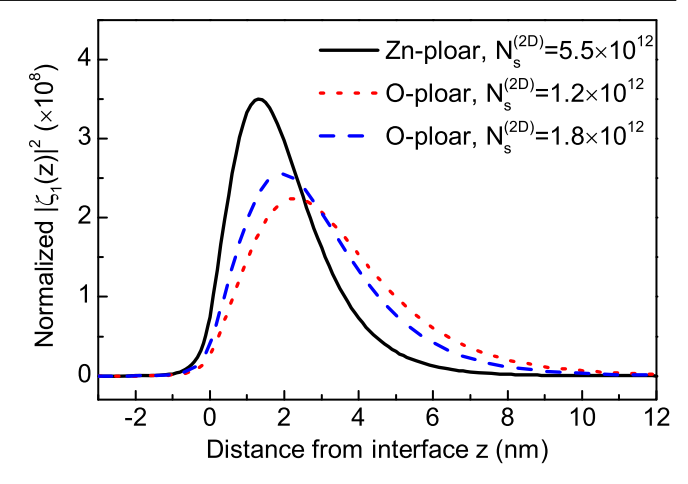


**Figure 1.** Calculated 2DEG wave functions for three different cases.  $N_s^{(2D)}$  in the legend is in units of cm<sup>-2</sup>.

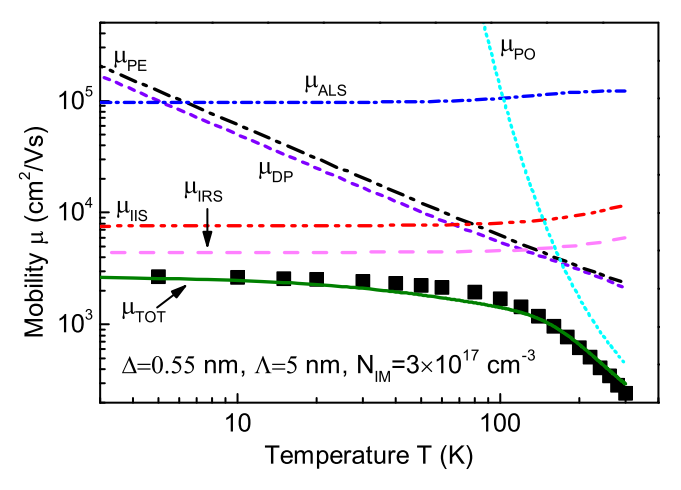


**Figure 2.** A Fit to the experimental data of Tampo *el al* [6]. The decomposed mobilities due to interface roughness scattering ( $\mu_{IRS}$ ), ionized impurity scattering ( $\mu_{IIS}$ ), alloy scattering ( $\mu_{ALS}$ ), acoustic DP scattering ( $\mu_{DP}$ ), acoustic PE scattering ( $\mu_{PE}$ ), PO phonon scattering ( $\mu_{PO}$ ), and the combined mobility ( $\mu_{TOT}$ ) are present. The solid squares represent the experimental data of Tampo *el al* [6].

temperature. The wave functions represented by the solid, dotted and dashed lines will be used in transport analyses for the Zn-polar ZnMgO/ZnO sample reported by Tampo *et al* [6], O-polar ZnO/ZnMgO samples B and C reported by Tsukazaki *et al* [5], respectively, in the following sections.

# 3.2. Electron transport in 2DEG

In the Zn-polar ZnMgO/ZnO heterostructure reported by Tampo *et al* [6], the sheet carrier density determined by Shubnikov–de Haas (SdH) measurement approaches the result determined by Hall measurement, and the Hall result is nearly independent of temperature, which implies that almost all electrons are confined in the 2DEG, thus the effect of parallel conduction on the electron transport is not important. We attempt to explain the electron mobility using the pure 2DEG transport theory presented in section 2.2. Figure 2 shows a fit to the experimental data of Tampo *et al* [6]. By

<sup>&</sup>lt;sup>b</sup> [33]

<sup>[34]</sup> 

<sup>[35]</sup> 

<sup>[36]</sup> 

<sup>[37]</sup> 

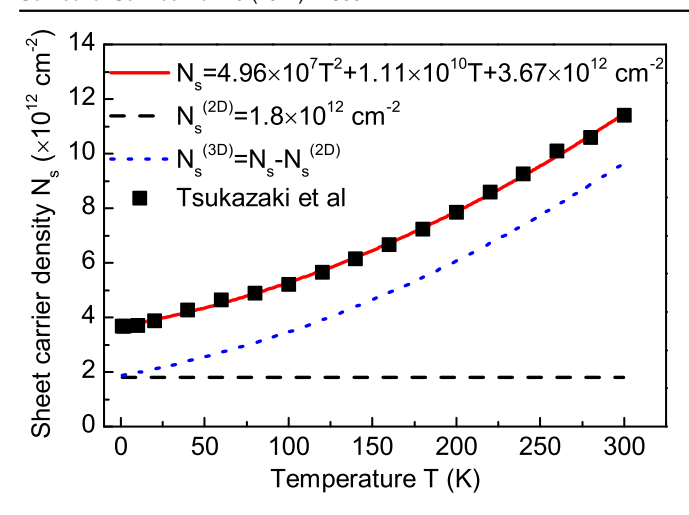


**Figure 3.** Sheet carrier density as a function of temperature. The solid squares represent the sheet carrier density for sample C of Tsukazaki *et al* [5].

setting the roughness parameters  $\Delta = 0.55$  nm and  $\Lambda = 5$  nm, and the ionized impurity density  $N_{\rm IM} = 3 \times 10^{17}$  cm<sup>-3</sup>, a good agreement is obtained between the theoretical and experimental results. The IRS and IIS dominate the mobility at low and moderate temperatures. The parameters for the IIS and IRS are independent, thus a good fit could be found using other parameter settings. An accurate evaluation of the relative importance of IIS and IRS relies on direct measurements of these parameters. The ALS is quite small, but this scattering is determined only by Mg composition and cannot be removed by improving crystal quality. The acoustic PE scattering is close to the DP scattering, but they have different density dependences. [39] The PO phonon scattering dominates the mobility at temperatures above 200 K.

The IIS is the most important scattering mechanism in bulk materials at low temperatures, but because the overlapping of electrons with impurities is small in heterostructure materials, the IIS may be relatively less important in 2DEG electron transport. In contrast, the IRS may be important, particularly in high density 2DEG [39].

### 3.3. Parallel conduction mechanism

Tsukazaki et al [5] observed SdH oscillations and quantum Hall effects in O-polar ZnO/ZnMgO heterostructures. The samples they measured have significant temperature dependence of the sheet carrier densities, implying the presence of parallel conduction in the ZnO thick layer. Figure 3 shows the extraction of the 2DEG and the bulk conduction components from the total sheet carrier density for sample C of Tsukazaki et al [5]. The total sheet carrier density is given by Hall measurement, which can be approximated  $N_{\rm s} = 4.96 \times 10^7 \, T^2 + 1.11 \times 10^{10} T + 3.67 \times 10^{12} \, {\rm cm}^{-2}$ . The 2DEG sheet carrier density,  $N_s^{(2D)} = 1.8 \times 10^{12} \,\mathrm{cm}^{-2}$ . derived from SdH measurement, is assumed independent of temperature. Thus, the sheet carrier density of bulk electrons  $N_{\rm s}^{\rm (3D)}$  can be given by  $N_{\rm s}^{\rm (3D)} = N_{\rm s} - N_{\rm s}^{\rm (2D)}$ . It can be seen from figure 3 that even at liquid helium temperatures the  $N_c^{(3D)}$  is

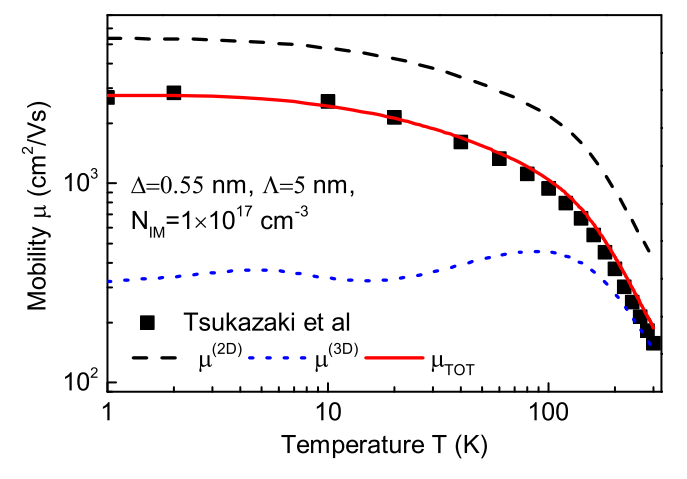


**Figure 4.** Mobility as a function of temperature. The solid squares represent the experimental data for sample C of Tsukazaki *et al* [5].

larger than the  $N_s^{(2D)}$ , implying that the bulk conduction is important in the electron transport in this heterostructure. As the temperature increases, the contribution of the bulk conduction to the electron transport will continuously increase.

We attempt to fit the electron mobility for this sample using the parallel conduction mechanism. The 2DEG mobility is calculated using the model presented in section 2.2; the bulk electron mobility is calculated considering the IIS, acoustic phonon scattering, and PO phonon scattering. The Brooks-Herring model, though very popular in studying the IIS of bulk electrons, will make incorrect predictions at low temperatures when the screening length becomes much shorter than the average separation distance of the impurities. Here, a modified Brooks-Herring model proposed by Takimoto [40] is used to calculate the IIS of bulk electrons, and the acoustic phonon scattering is calculated according to Yang et al [14], and the PO phonon scattering is calculated by solving the Boltzmann equation directly [41]. After the 2DEG mobility,  $\mu^{(2D)}$ , and the bulk electron mobility,  $\mu^{(3D)}$ , are calculated, a combined mobility is given by  $\mu_{\rm TOT} = y \cdot \mu^{\rm (2D)} + (1-y) \cdot \mu^{\rm (3D)}$ , where  $y = N_{\rm s}^{\rm (2D)}/N_{\rm s}$  is the 2DEG density fraction.

Figure 4 shows a fit to the experimental data for sample C of Tsukazaki *et al* [5]. By taking into account the 2DEG and the bulk conduction paths, the calculated results are in good agreement with the experimental data. The theoretical mobilities in the 2DEG and in the ZnO thick layer are calculated using the same parameters, i.e.  $N_{\rm IM}=1\times10^{17}\,{\rm cm^{-3}},$   $\Delta=0.55\,{\rm nm},$  and  $\Lambda=5\,{\rm nm}.$  Note that there is a slight oscillation in the  $\mu^{\rm (3D)}$  at lower temperatures; this is because in the IIS, due to higher density of bulk electrons in sample C, Takimoto's modification cannot completely overcome the strong screening problem in the Brooks–Herring model.

We use the parallel conduction mechanism to fit another experimental data of Tsukazaki *et al* [5]. It can be seen from figure 5 that a good fit is obtained by setting  $N_{\rm IM} = 5.8 \times 10^{16} \, {\rm cm}^{-3}, \ \Delta = 0.55 \, {\rm nm}, \ \Lambda = 5 \, {\rm nm},$  demonstrating the validity of the parallel conduction mechanism.

In the published literature, the DP constant D of ZnO is usually treated as a fitting parameter ranging from 3.8 to

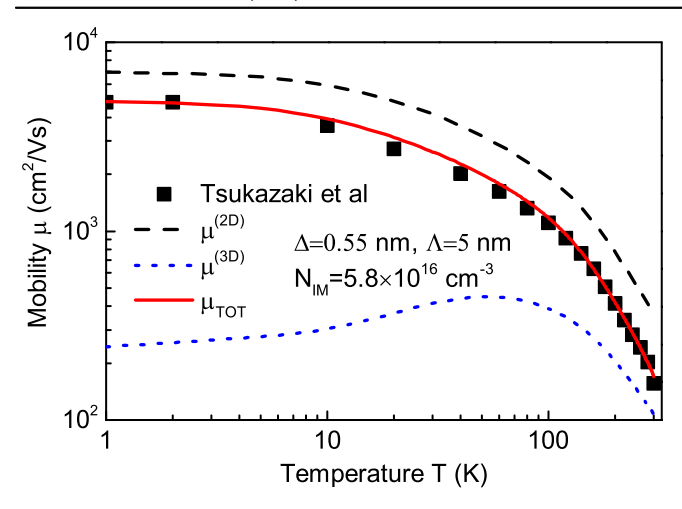


**Figure 5.** Mobility as a function of temperature. The solid squares represent the experimental data for sample B of Tsukazaki *et al* [5].

15 eV [16, 36, 38]. When using the curve fitting method to determine D value, both measurement errors and other inaccurate parameter estimates could cause a large variation in the D value. The accurate determination of D requires accurate experimental data measured in high-pure, defect-free ZnO materials and more theoretical studies. In this study, all three sets of experimental data are well fitted using D = 15 eV, and other intrinsic parameters also remain unchanged.

# 4. Conclusions

In this study, the electron transport in ZnMgO/ZnO heterostructures is studied using numerical 2DEG wave functions. The experimental data reported by Tampo et al [6] are satisfactorily explained using the pure 2DEG transport theory. It is found that the interface roughness and ionized impurity scatterings dominate the electron mobility at low and moderate temperatures. At room temperature the polar optical phonon scattering is the most important scattering mechanism. For the heterostructures exhibiting obvious parallel conduction characteristics, the electron transport is contributed by two parallel conduction paths in the 2DEG at the ZnMgO/ZnO interface and in the ZnO thick layer. The parallel conduction mechanism is used to fit the experimental data of Tsukazaki et al [5]. Each set of experimental data can be explained satisfactorily using our theory without adjusting any intrinsic parameter values.

# **Acknowledgements**

This work was supported by the National Natural Science Foundation of China under Grant Nos. 61176018 and 60876042, and the National High Technology Research and Development Program of China (863 Program) under Grant No. SQ2013GX04D00825.

### References

- [1] Özgür Ü, Alivov Ya I, Liu C, Teke A, Reshchikov M A, Doğan S, Avrutin V, Cho S-J and Morkoç H 2005 J. Appl. Phys. 98 041301–404
- [2] Koike K, Hama K, Nakashima I, Takada G, Ozaki M, Ogata K, Sasa S, Inoue M and Yano M 2004 Jpn. J. Appl. Phys. 43 L1372-5
- [3] Ye J D, Gu S L, Li F, Zhu S M, Zhang R, Shi Y, Zheng Y D, Sun X W, Lo G Q and Kwong D L 2007 Appl. Phys. Lett. 90 152108–10
- [4] Akasaka S, Tsukazaki A, Nakahara K, Ohtomo A and Kawasaki M 2011 Jpn. J. Appl. Phys. 50 080215–7
- [5] Tsukazaki A, Ohtomo A, Kita T, Ohno Y, Ohno H and Kawasaki M 2007 Science 315 1388–91 (and the supporting online material: www.sciencemag.org/cgi/content/full/ 1137430/DC1)
- [6] Tampo H et al 2008 Appl. Phys. Lett. 93 202104-6
- [7] Fang F F and Howard W E 1966 Phys. Rew. Lett. 16 797-9
- [8] Ando T 1982 J. Phys. Soc. Jpn. 51 3900-7
- [9] Kawamura T and das Sarma S 1992 Phys. Rev. B 45 3612-27
- [10] Lisesivdin S B, Acar S, Kasap M, Ozcelik S, Gokden S and Ozbay E 2007 Semicond. Sci. Technol. 22 543-48
- [11] Li Q, Zhang J, Chong J and Hou X 2013 Appl. Phys. Express 6 121102–4
- [12] Kaschner A et al 2002 Appl. Phys. Lett. 80 1909–11
- [13] Van de Walle C G 2001 Physica B 308-310 899-903
- [14] Yang X, Xu C and Giles N C 2008 J. Appl. Phys. 104 073727–32
- [15] Baghani E and O'Leary S K 2013 J. Appl. Phys. 114 023703-6
- [16] Bertazzi F, Bellotti E, Furno E and Goano M 2009 J. Electron. Mater. 38 1677–83
- [17] Tampo H et al 2009 Appl. Phys. Lett. 94 242107–9
- [18] Li Q, Zhang J, Meng L and Hou X Phys. Status Solidi B 251 755–60
- [19] Massidda S, Resta R, Posternak M and Baldereschi A 1995 Phys. Rev. B 52 R16977–80
- [20] Malashevich A and Vanderbilt D 2007 Phys. Rev. B 75 045106–10
- [21] Lee K S, Yoon D H, Bae S B, Park M R and Kim G H 2002 ETRI journal 24 270-9
- [22] Jogai B 2002 J. Appl. Phys. 91 3721-9
- [23] Coleridge P T 1990 Semicond. Sci. Technol. 5 961-6
- [24] Li J M, Wu J J, Han X X, Lu Y W, Liu X L, Zhu Q S and Wang Z G 2005 Semicond. Sci. Technol. 20 1207–12
- [25] Lisesivdin S B, Yildiz A, Balkan N, Kasap M, Ozcelik S and Ozbay E 2010 J. Appl. Phys. 108 013712–8
- [26] Quang D N, Tung N H, Tuoc V N, Minh N V, Huy H A and Hien D T 2006 Phys. Rev. B 74 205312–25
- [27] Yano M, Hashimoto K, Fujimoto K, Koike K, Sasa S, Inoue M, Uetsuji Y, Ohnishi T and Inaba K 2007 J. Cryst. Growth 301-302 353-7
- [28] Janotti A, Segev D and van de Walle C G 2006 Phys. Rev. B 74 045202–10
- [29] Fishman G and Calecki D 1991 Phys. Rev. B 43 11581-5
- [30] Ishibashi A, Takeishi H, Mannoh M, Yabuuchi Y and Ban Y 1996 J. Electron. Mater. 25 799–803
- [31] Price P J 1981 Ann. Phys. 133 217-39
- [32] Martin L P and Rosen M 1997 J. Am. Ceram. Soc. 80 839-46
- [33] Fukumura T, Jin Z, Kawasaki M, Shono T, Hasegawa T, Koshihara S and Koinuma H 2001 Appl. Phys. Lett. 78 958–60
- [34] Bertazzi F, Goano M and Bellotti E 2007 *J. Electron. Mater.* **36** 857–63
- [35] Hutson A R 1961 J. Appl. Phys. 32 2287-92
- [36] Rode D L 1975 Semiconductors and Semimetals (Low-field Electron Transport vol 10) ed R K Willardson and A C Beer (New York: Academic) p 84

- [37] Kobiakov I B 1980 Solid State Commun. 35 305–10
  [38] Look D C, Reynolds D C, Sizelove J R, Jones R L, Litton C W, Cantwell G and Harsch W C 1998 Solid State Commun. 105
- [39] Zanato D and Gokden S 2004 Balkan N, Ridley B K and Schaff W J Semicond. Sci. Technol. 19 427-32
- [40] Takimoto N 1959 J. Phys. Soc. Jpn. 14 1142-58
- [41] Nag B R 1980 Electron transport in compound semiconductors (Berlin: Springer) pp 129-70